Applied Mathematical Modelling 39 (2015) 363–382

Contents lists available at ScienceDirect

Applied Mathematical Modelling

journal homepage: www.elsevier.com/locate/apm

A SPH model for the simulation of free surface granular flows in a dense regime

Lorenzo Minatti [a,*], Enio Paris [b]

[a] CERAFRI, Civil and Environmental Engineering Department, University of Florence, Italy
[b] Civil and Environmental Engineering Department, University of Florence, Italy

ARTICLE INFO

Article history:
Received 18 July 2013
Received in revised form 1 March 2014
Accepted 27 May 2014
Available online 8 June 2014

Keywords:
Smoothed Particles Hydrodynamics
Granular flows
Viscosity regularisation

ABSTRACT

Smoothed Particle Hydrodynamics (SPH) is a particle-based Lagrangian numerical method, particularly suitable for modeling free surface flows of fluids with different constitutive equations. In this work, a SPH model is developed to solve flow problems of granular matter flowing in a dense regime, featuring a constitutive equation proposed by Pouliquen et al. (2006) [17] and Jop et al. (2006) [18].

The problem of resolving the flow close to static conditions has been solved by introducing a weak compressibility for the grains: this leads to a third order algebraic equations to be solved for computing granular material density. A new viscosity regularisation method, suitable for any visco-plastic fluid with varying yield stress has been developed, in order to reproduce stopping flow and static conditions.

Validation of the model has been performed by solving the simple uniform granular flow problem, for which the solution is known analytically and by reproducing a set of experimental data on granular columns collapses by Lube et al. (2004) [19].

1. Introduction

Numerical simulation of free surface flows is often a complex task, especially within the framework of grid-based methods, even though successful approaches such as the Volume of Fluid method [1] have been proposed in the past. Meshless particle methods on the other hand, seem to provide a more efficient way to deal with free surfaces issues.

Among various methods of this kind, Smoothed Particle Hydrodynamics (SPH) proved to be successful in many cases. Firstly proposed by Gingold and Monaghan [2] and by Lucy [3] for astrophysical applications, SPH was employed to simulate free surface flows by Monaghan [4], Ferrari et al. [5] and Violeau and Issa [6] to name a few.

SPH is also a very versatile method for implementing different constitutive equations: Rodriguez-Paz and Bonet [7], Laigle et al. [8], Pasculli et al. [9] and Minatti and Pasculli [10] performed SPH simulations of mudflows using Bingham-type fluids, while Bui et al. [11] used elastic–plastic relations to model soil failure flows.

A comprehensive overview of the numerous applications of SPH, together with a general review of the method can be found in Monaghan [12,13], Liu and Liu [14] and Violeau [15].

The purpose of this work is to develop a SPH-based model for the simulation of complex free surface dense granular flows, taking advantage of the afore mentioned properties of the method. Granular flows have many applications in the industrial

* Corresponding author. Tel.: +39 55 4796458; fax: +39 55 4796494.
E-mail address: lminatti@dicea.unifi.it (L. Minatti).

http://dx.doi.org/10.1016/j.apm.2014.05.034
0307-904X/

field, ranging from pharmaceutical to semiconductor industries where, according to Richard et al. [16] granular materials are *'the second-most manipulated material'* after water. They are of great interest in the civil engineering field too: during the last years, attention has increasingly focused on the hazard represented by the solid material carried by rivers during extreme events.

A general constitutive equation for granular matter, suitable for any kind of flow, is not available in scientific literature yet. Nevertheless, a number of constitutive equations have been proposed, each one of them being able to correctly reproduce specific classes of granular flows.

Attention has been focused on the constitutive equation proposed by Pouliquen et al. [17] and Jop et al. [18] which can be applied to a fairly wide class of flows within a dense regime, where granular interactions are dominated by friction.

The proposed SPH model employs a new method for pressure calculation, necessary in order to resolve the flow at low strain rates. The method is based on the introduction of weak compressibility for the grains and is specific to the constitutive equations under investigation. The SPH model also features a new viscosity regularisation method, suitable for any visco-plastic fluid with variable yield stress.

In Section 2 the equations describing the physics of the system are introduced, together with the employed constitutive equation. A general overview of the SPH method is then provided in Section 3. The proposed SPH model is introduced in Section 4. Validation of the model is performed in Section 5 by reproducing a simple sheet flow test case for which the analytical steady state solution is known and by reproducing experimental measurements of granular material collapses by Lube et al. [19]. Final conclusions regarding the model and its performances are drawn in Section 6.

2. Governing equations

The most widely used approaches to model granular matter are usually related either to continuum or to granular mechanics (Computational Granular Dynamics [20]). In the present work, a "continuum" approach, where granular matter is treated as an equivalent fluid moving with a flow field having the same features as the one of the original material, has been employed.

Therefore, the equations we resort to are the mass conservation and momentum equations of classical mechanics, written in their local Lagrangian form:

$$\frac{D\rho}{Dt} = -\rho\nabla\cdot\underline{v}, \tag{1}$$

$$\frac{D\underline{v}}{Dt} = \underline{g} - \frac{\nabla p}{\rho} + \frac{\nabla\cdot\underline{\underline{\tau}}}{\rho}, \tag{2}$$

where ρ is the fluid density, $\underline{v}$ is the velocity field, $\underline{g}$ is the gravity acceleration, p is the isotropic pressure, $\underline{\underline{\tau}}$ is the deviatoric part of the stress tensor, ∇ is the gradient operator and $\nabla\cdot$ is the divergence operator. D/Dt indicates the Lagrangian derivative operator, defined as:

$$\frac{D(\cdot)}{Dt} = \frac{\partial(\cdot)}{\partial t} + \nabla(\cdot)\underline{v}. \tag{3}$$

In the case of an incompressible fluid, no density variations occur. Incompressibility condition forces the fluid to move with a divergence free velocity field and pressure is obtained by solving a Poisson PDE [22]. Otherwise, in the case of compressible or weakly compressible fluids, pressure is calculated from density trough an equation of state (EOS) of the form $p = f(\rho)$.

The deviatoric stress tensor $\underline{\underline{\tau}}$ is calculated from the constitutive equation, whose expression depends on the material under study. A wide class of constitutive equations relates the stress tensor of the material to its strain rate tensor, whose components are $\epsilon^{\alpha\beta} = \frac{1}{2}(\partial v^{\alpha}/\partial x^{\beta} + \partial v^{\beta}/\partial x^{\alpha})$ in a cartesian frame of reference. The constitutive equation for a general viscous compressible fluid, can be written as in Landau and Lifshitz [21]:

$$\underline{\underline{\tau}} = 2\eta\left(\underline{\underline{\epsilon}} - \frac{\nabla\cdot\underline{v}}{3}\underline{\underline{I}}\right) + (\xi\nabla\cdot\underline{v})\underline{\underline{I}}, \tag{4}$$

where η is the shear viscosity, responsible for the stress associated to the non isotropic part of the strain rate tensor, ξ is the bulk viscosity, acting only on compressible fluids by dampening volume variations and $\underline{\underline{I}}$ is the unit tensor. If η and ξ are constant, the fluid is usually referred to as a Newtonian fluid; if η or ξ vary in space, the fluid is usually referred to as a non-Newtonian fluid.

Devising a constitutive equation that is able to correctly reproduce the dynamics of an assembly of particles is a difficult task. So far, it does not exist a law able to describe the rheology of granular matter regardless of its flowing conditions. All the available constitutive equations have a limited range of validity which depends, among others variables, on velocity, average spacing of grains during motion, elastic properties of grains.

In the case of cohesionless granular material, if the grain size d is sufficiently large (typically $d > 250\ \mu m$) and the interstitial fluid is not too viscous, interactions between grains are dominated by contact interactions [22]. In this case, the

mechanical properties of the material depend only on momentum transfer during grains collisions or frictional contacts. Other variables, such as capillary forces or viscous interactions with interstitial fluid can be neglected. In nature, situations that are relevant to these conditions are not uncommon. Under these assumptions, granular flows are usually classified into three regimes [22,17] according to the nature of the main interaction between grains. Different constitutive equations have been proposed for each one of these regimes.

When velocities are very low and grains inertia is negligible, a quasi-static regime occurs. Within this regime, soil plasticity models have been successfully used in the SPH framework [11]. On the other hand, when the flow intensity is very high and grains are apart from each other, a collisional regime occurs. Interactions are dominated by collisions between grains and it becomes crucial to provide a correct estimate of energy losses during such collisions in order to devise an efficient constitutive law for the material. Within this regime, the granular matter behavior is similar to the one of a gas and kinetic theories based approaches have been developed [23]. In the intermediate regime, herein called *dense* regime, grains inertia becomes important while particles still experience enduring contact, which makes it impossible to use kinetic theories. The studies of Pouliquen et al. [17] and Jop et al. [18] are focused on this regime.

The basic assumption of the theory stems from results obtained by Da Cruz et al. [24] through molecular dynamics simulations, where in the dense regime of a plane granular flow, it is possible to assume a linear relation between the shear stress τ and the confining pressure p:

$$\tau = \mu p, \tag{5}$$

The proportionality coefficient μ depends on a non dimensional number i, defined as the *inertial number* by Da Cruz et al. [24] which is provided by the following equation [25]:

$$i = \frac{\dot{\gamma} d}{\sqrt{\frac{p}{\rho_s}}}, \tag{6}$$

where $\dot{\gamma} = \sqrt{2\left(\underline{\underline{\epsilon}} : \underline{\underline{\epsilon}}\right)}$ is the strain rate tensor module (The symbol ":" indicates the Frobenius inner product) and ρ_s is the density of the grains material.

A small value of i, indicating high pressure or low strain rates, corresponds to the quasi-static regime of granular flows, where grains inertia is negligible. A high value of i, occurring at high strain rates or at low pressure corresponds to the collisional regime of flow, where kinetic theories should be employed. The collisional regime is usually considered to occur for $i > 0.3$, see Pouliquen et al. [17].

The μ coefficient locally depends on the inertial number: an hypothesis on the form of $\mu(i)$ has been firstly proposed by Jop et al. [25]:

$$\mu = \mu_s + \frac{\mu_2 - \mu_s}{1 + \frac{i_0}{i}}, \tag{7}$$

where μ_s is the lower bound of μ corresponding to the fluid at rest condition $(i = 0)$, μ_2 is the upper bound of μ, i_0 is a reference value for the inertial number (see Section 2.1).

The volume fraction ϕ, defined as the volume occupied by grains in the unit volume, should decrease as the flow moves from a quasi-static regime towards a collisional one. According to the physical meaning of the inertial number, the following functional form has been proposed by Pouliquen et al. [17]:

$$\phi = \phi_{max} - (\phi_{max} - \phi_{min})i, \tag{8}$$

where ϕ_{max} is the upper bound for the volume fraction, occurring when there is no flow, its value depending on the grains size and shape, ϕ_{min} is the lower bound for the volume fraction: it should represent the threshold below which the grains are too far apart from each other to model the granular material as an equivalent single fluid rather than an assembly of particles. Typically the values $\phi_{max} = 0.6$ and $\phi_{min} = 0.5$ are used (see Pouliquen et al. [17]).

The volume fraction ϕ establishes also the relation between the bulk density of the continuum ρ and the density of the granular material ρ_s:

$$\rho = \phi \rho_s. \tag{9}$$

Eq. 5, provides the constitutive equation for the "granular fluid" in a 1D case. It has been extended to a 2D or 3D case in the following way by Jop et al. [18] and Pouliquen et al. [17]:

$$\tau^{\alpha\beta} = 2\frac{\mu(i)p}{\dot{\gamma}}\epsilon^{\alpha\beta}. \tag{10}$$

By confrontation with Eq. (4), it can be seen how Eq. (10) represents the constitutive equation of an incompressible non-Newtonian fluid, with no bulk viscosity and with the following pressure dependent shear viscosity:

$$\eta = \frac{\mu(i)p}{\dot{\gamma}}. \tag{11}$$

Despite single grains are supposed to be rigid and incompressible (ρ_s is constant), the granular pack is indeed compressible to a certain extent, at least when it starts moving from a rest position. When the granular material starts moving, its inertial number i increases from zero and according to Eqs. (8) and (9), its bulk density ρ decreases through changes in ϕ, which is a measure of how the grains are close to each other during the motion. Eq. (10) should apply to an incompressible fluid but the variations of ϕ are small and an incompressible assumption is however possible in the dense regime, see Forterre and Pouliquen [26].

Eq. (10) is the constitutive equation of a visco-plastic fluid, whose yield stress τ_y is:

$$\tau_y = \mu_s p \tag{12}$$

At the yield point, viscosity diverges to infinity and the fluid starts to behave like a rigid body.

Eqs. (4), (7), (8) and (11) define the constitutive relations of the granular matter in the dense regime. The complete set of equations describing the flow of granular matter in this regime are summarized below:

$$\begin{aligned}
&\frac{D\rho}{Dt} = -\rho \nabla \cdot \underline{v},\\
&\frac{D\underline{v}}{Dt} = \underline{g} - \frac{\nabla p}{\rho} + \frac{\nabla \cdot 2\eta \underline{\underline{\epsilon}}}{\rho},\\
&\eta = \frac{\mu p}{\dot{\gamma}},\\
&\dot{\gamma} = \sqrt{2\left(\underline{\underline{\epsilon}} : \underline{\underline{\epsilon}}\right)},\\
&\mu = \mu_s + \frac{\mu_2 - \mu_s}{1 + \frac{i_0}{i}},\\
&i = \frac{\dot{\gamma} d}{\sqrt{\frac{p}{\rho_s}}},\\
&\rho = \phi \rho_s,\\
&\phi = \phi_{max} - (\phi_{max} - \phi_{min}) i.
\end{aligned} \tag{13}$$

Please note that the momentum equation above has been written neglecting the velocity field divergence related terms. Such terms have a minor importance in the momentum equation when the fluid is weakly compressible and completely disappear when it is incompressible.

In a 2D case the model is made of a set of 9 scalar equations (note that the 2nd equation is vectorial) which can be solved with respect to the following 9 scalar unknowns: (ρ, $\underline{v}$, p, η, μ, $\dot{\gamma}$, i, ϕ). The quantities ρ_s and d in system (13) are known and summarize the grains properties.

In literature, there exist studies where granular flows equations based on kinetic theories are investigated (this is often the case in which the flow is occurring at a collisional regime). Woodhouse et al. [27] found existence domains of steady state solutions for inclined planar chute flows. Kumaran [28] found, in the case of planar flows down inclined planes, that the existence of boundary layer solutions is related to the dependence of volume fraction in the outer flow region on the angle of inclination of the plane. Nevertheless, as far as existence of solutions for the highly nonlinear system in the present work is concerned, studies of this kind do not exist to the knowledge of the authors.

In Section 4, some modifications will be introduced on system (13). They are necessary in order to address some issues arising when the flow is close to the static regime. A first one is related to the shear viscosity of Eq. (4), which becomes very large when approaching such conditions, leading to excessively small time steps (see Eq. (39)). The other one is related to pressure computation in areas where the granular matter is flowing at low strain rates.

2.1. Determination of material-dependent parameters in the constitutive equation

Reviews of available experimental data for the constitutive equation under study can be found in Pouliquen [29], Pouliquen and Forterre [30], Forterre and Pouliquen [31], GDR MiDi [22] and in Pouliquen et al. [17]. Another extensive set of experimental data can be found in Borzsonyi and Ecke [32].

Most of the experiments were carried out on granular flows of glass beads ($d = 0.5$ mm size) and sand ($d = 0.8$ mm size). Although most of the data refer to experiments carried out in planar flow conditions, it is possible to start from them in order to devise the most appropriate values for the parameters of the constitutive equation. In the present work, such values have been used to simulate more complex flows, similarly to GDR MiDi [22], where discrete particle simulations were carried out to simulate planar, axisymmetric and free surface flows.

During experiments with granular material released down an inclined plane, it was found that when the flow of the grains down the plane was stopped, for example by lowering the channel inclination, a residual layer of grains of thickness H_{stop} remained at rest on the plane. The following experimental relations were found (see Forterre and Pouliquen [31]):

$$\frac{V}{\sqrt{gH}} = -\gamma + \beta\frac{H}{H_{stop}}, \tag{14}$$

$$H_{stop}(\theta) = L\left(\frac{\mu_2 - \mu_s}{\mu - \mu_s} - 1\right), \tag{15}$$

where V is the average velocity of the resulting flow, H is the thickness of the flowing layer, representing a scaling length of the problem and $\mu = \tan\theta$ is the friction related to plane inclination θ. The values for the remaining parameters L, γ, β in Eqs. (14) and (15) depend on the material and are reported in Table 1 for glass beads and sand.

By using Eqs. (14), (15) and (6) it is possible to break Eq. (7) down into the following expression:

$$\mu = \mu_s + \frac{\mu_2 - \mu_s}{1 + \left(\frac{\beta d}{L}\right) \Big/ \left(\frac{\gamma d}{H} + \frac{dV}{H\sqrt{gH}}\right)}. \tag{16}$$

Jop et al. [25] found the following expression for the parameter i_0 of Eq. (7):

$$i_0 = \frac{5\beta d}{2L\sqrt{\phi\cos\theta}}, \tag{17}$$

by using Eq. (16) and information derived from experimental evidence of V scaling with the 3/2 power of the flow reference length H. By using data from glass beads (1st column of Table 1) and and average values for the quantities $\phi = 0.60$ and $\theta = 25^\circ$ they found the value $i_0 = 0.279$.

In order to devise the most appropriate value of i_0 for sand, a similar action is performed on Eq. (16) using either the values in the 2nd or 3rd column of Table 1. The following expression can then be found:

$$\mu = \mu_s + \frac{\mu_2 - \mu_s}{1 + \frac{i_0}{i + 2.61 d/H}}, \tag{18}$$

with $i_0 = 1.09$ for 0.8 mm sand and $i_0 = 2.65$ for 0.4 mm sand.

While Eq. (18) is exact for free surface planar flows, with H representing the flowing layer thickness, it is possible to attempt to use it in the case of more complex sand granular flows, assuming H as a scaling length of the flow.

The dependency of μ on the ratio H/d can be investigated by calculating the relative error committed on the estimation of μ when the $2.61d/H$ term of Eq. (18) is dropped. The results are plotted in Fig. 1 as a function of i.

It can be seen from Fig. 1 that the largest errors occur when $i \approx 0$. For increasing i, errors decrease regardless of H/d. For increasing H/d and constant i, errors decrease as well. If the ratio H/d ratio is sufficiently large such errors are negligible for every value of the inertial number and Eq. (7), which is more simple and does not exhibit explicit dependency on the length scale of the problem H, can be used instead of Eq. (18).

3. Overview of SPH

SPH is a fully meshless method in which the fluid domain is discretised into a set of particles, each one representing a finite area and carrying flow information. Interpolation of functions and derivatives appearing in the equations to be solved is performed over a set of particles, rather than on mesh points as it happens in other methods such as finite differences or finite volumes.

SPH is a Lagrangian method: particles are moved in the computational domain according to their velocities at each time step of the simulation, providing an automatic and physically based update of the interpolation nodes.

The features of SPH allow the straightforward handling of fluid flow problems involving free surfaces and strong deformations such as dam break type flows. Furthermore, the Lagrangian nature of the method allows the direct integration of equations with time derivatives cast into Lagrangian form, like Eqs. (1) and (2). This provides a simplification, avoiding the need to find a suitable numerical approximation to the advective terms that would appear in the equations if eulerian expression for time derivatives were used.

Table 1
Experimental values for the parameters of constitutive equation.

	Glass beads ($d = 0.5$ mm) from [22]	Sand ($d = 0.8$ mm) from [22]	Sand ($d = 0.4$ mm) from [23]
μ_s ()	$\tan(20.90^\circ)$	$\tan(27.00^\circ)$	$\tan(30.50^\circ)$
μ_2 ()	$\tan(32.76^\circ)$	$\tan(43.40^\circ)$	$\tan(51.30^\circ)$
L/d ()	1.65	2.03	0.83
γ ()	0.00	0.77	
β ()	0.136	0.650	

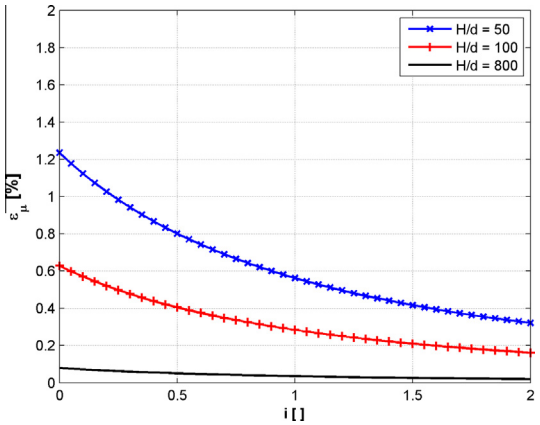

Fig. 1. Relative error committed neglecting the $2.61d/H$ term of Eq. (18) plotted as a function of i. All the curves are plotted for $\mu_2/\mu_s \approx 1.5$ and $i_0 = 2.65$.

In the present section we summarize the basic features of the method that are relevant to the present work. More detailed reviews of the method can be found in Monaghan [12,13], Liu and Liu [14] and Violeau [15].

3.1. Basic concepts

It is well known that a generic continuous compactly supported function of space $f(\underline{r})$ can be reproduced by means of a convolution integral with a delta function δ:

$$f(\underline{r}) = \int f(\underline{r}') \cdot \delta(\underline{r} - \underline{r}') d\underline{r}'. \tag{19}$$

In SPH, the delta function is replaced by a smooth kernel function W, with a compact support domain Ω_r. The kernel function is even and bell-shaped, having its peak at the center of the support domain and vanishing outside of it. It also has to satisfy further properties such as normalization and delta function convergence. The interested reader is referred to the references provided at the beginning of the present section.

The support domain is a $\underline{r}$-centered, usually circular set, whose radius is multiple of a scaling length h, named *smoothing length*. The smoothing length represents the discretisation scale of SPH approximations, playing a similar role as grid spacing in mesh based methods.

The kernel used for the simulations in the present work is the C4 (quartic) Wendland kernel [33]. Such kernel has good smoothness properties and has previously been used by Monaghan and Kajtar [34]. Its expression in a 2D case is as follows:

$$W(\underline{r} - \underline{r}', h) = \frac{7}{64\pi h^2} \cdot \begin{cases} (1+2R)(2-R)^4 & \text{for } 0 \leqslant R < 2, \\ 0 & \text{for } R \geqslant 2. \end{cases} \tag{20}$$

where $R = |\underline{r} - \underline{r}'|/h$.

The convolution integral of a compact supported function with a kernel produces an approximation of the function itself, which we indicate with the symbol $\langle f(\underline{r}) \rangle$:

$$\langle f(\underline{r}) \rangle = \int_{\Omega_r} f(\underline{r}') \cdot W(\underline{r} - \underline{r}') d\underline{r}'. \tag{21}$$

By using the Gauss–Green formula and assuming $f(\underline{r})$ to be differentiable, it is possible to obtain an approximation for its gradient:

$$\langle \nabla f(\underline{r}) \rangle = \int_{\partial(\Omega_r \cap D)} f(\underline{r}') \cdot W(\underline{r} - \underline{r}') d\underline{r}' - \int_{\Omega_r} f(\underline{r}') \cdot \nabla' W(\underline{r} - \underline{r}') d\underline{r}'. \tag{22}$$

with $\nabla' W$ indicating differentiation with respect to $\underline{r}'$ variable, ∂ indicating the set boundary, D indicating the computational domain. By using Eq. (22) it is possible to shift the gradient operator from the function to the kernel. Note that if the set Ω_r is fully included into the computational domain, then Eq. (22) reduces to:

$$\langle \nabla f(\underline{r}) \rangle = -\int_{\Omega_r} f(\underline{r}') \cdot \nabla' W(\underline{r} - \underline{r}') d\underline{r}'. \tag{23}$$

Eqs. (21) and (23) represent the starting point from which SPH formulations are derived. It is worth mentioning that in many SPH formulations the $\int_{\partial\Omega_r}$ of Eq. (22) term is neglected even when Ω_r is not fully included in the computational domain (for example close to a rigid boundary).

Integrals in the previous formulas are numerically interpolated at particles locations and substituted by particles summations. If the particle located at the $\underline{r}$ position is indicated with the i label, and the generic particle located inside the $\underline{r}$-centered support domain Ω_r is indicated with the j label, then Eqs. (21) and (23) respectively take the form:

$$\langle f(\underline{r}_i)\rangle = \sum_{j=1}^{n} f(\underline{r}_j)\cdot W(\underline{r}_i - \underline{r}_j)\delta A_j, \tag{24}$$

$$\langle \nabla f(\underline{r}_i)\rangle = -\sum_{j=1}^{n} f(\underline{r}_j)\cdot \nabla_j W(\underline{r}_i - \underline{r}_j)\delta A_j, \tag{25}$$

where summations are extended to the n particles located within the support domain of particle i, δA_j denotes the area (or volume in 3D) associated with the particle j and ∇_j indicates that gradients are calculated with respect to coordinate $\underline{r}_j$. From now on, the symbol $\langle\rangle$ will be dropped to simplify the notation.

3.2. Momentum and mass conservation equations

There is no unique way to discretise mass conservation and momentum equations with SPH. In the present work the following formulations have been used, respectively:

$$\frac{D\rho_i}{Dt} = \sum_{j=1}^{n} \underline{v}_{ij}\cdot\nabla_i W_{ij} m_j, \tag{26}$$

$$\frac{D\underline{v}_i}{Dt} = \underline{g} - \sum_{j=1}^{n} m_j\left(\frac{p_i}{\rho_i^2}+\frac{p_j}{\rho_j^2}\right)\nabla_i W_{ij} + \sum_{j=1}^{n} 8\left(\frac{2\eta_i\eta_j}{\eta_i+\eta_j}\right)\frac{(\underline{v}_{ij}\cdot\underline{r}_{ij})\nabla_i W_{ij}}{r_{ij}^2\rho_i\rho_j} m_j, \tag{27}$$

where the area associated to single particle has been written as $\delta A_j = m_j/\rho_j$, m_j being the mass associated to particle j, $\underline{v}_{ij} = \underline{v}_i - \underline{v}_j$, $\underline{r}_{ij} = \underline{r}_i - \underline{r}_j$, $r_{ij}^2 = |\underline{r}_i - \underline{r}_j|^2$.

Eq. (26) has 0th order consistency as its right hand side (RHS) vanishes when the velocity field is constant.

The first term in the sum on the RHS of Eq. (27) is the SPH approximation for pressure gradient in the momentum equation. It does not provide 0th order consistency as it computes non zero gradients for constant pressure fields. The second term in the sum models viscous interactions. It provides 0th order consistency as it does not compute any viscous interaction between particles in the case of constant velocity fields. Furthermore, in the case of rigid body motion, with $\underline{v}_{ij} = \underline{\omega}\times\underline{r}_{ij}$, it turns out that $\underline{v}_{ij}\cdot\underline{r}_{ij} = 0$ as the velocity difference is a tangential vector and therefore particles do not exchange shear forces. Eq. (27) can properly handle space-varying viscosity (see Cleary [35]): it is therefore possible to use it for non-Newtonian fluids flows modeling.

The employment of a poorly accurate formulation for the pressure gradient in Eq. (27) introduces extra numerical diffusivity into the model, compared to the one introduced by more accurate formulations. Another effect is the one of computing non zero pressure gradients for constant pressure fields, thus producing numerical inter-particles forces. On the other hand, formulations with at least 0th order consistency can correctly compute spatial gradients of constant fields. This drawback in the pressure gradient formulation does not affect SPH abilities at modeling fluids at rest, at least when pressure is calculated from density through an EOS, as particles arrange their positions triggering density variations that offset pressure field imbalances (see the static tank test case in [34] as an example).

It is possible to prove that Eq. (27) allows both linear and angular momentum conservation. In order to do that, first we notice that, being the kernel an even function, its gradient in a 2D case is radially directed and can be written as:

$$\nabla_i W_{ij} = F(|\underline{r}_{ij}|)\cdot\underline{r}_{ij}, \tag{28}$$

where F is a negative function of inter-particle distance.

With no external forces, the time derivative for the linear momentum $\underline{Q}$ of the system of particles can be expressed starting from Eq. (27), with N indicating the total number of particles in the system:

$$\begin{aligned}\frac{D\underline{Q}}{Dt} &= \sum_{i=1}^{N} m_i\frac{D\underline{v}_i}{Dt} = -\sum_{i,j=1}^{n} m_i m_j\left(\frac{p_i}{\rho_i^2}+\frac{p_j}{\rho_j^2} - 8\left(\frac{2\eta_i\eta_j}{\eta_i+\eta_j}\right)\frac{\underline{v}_{ij}\cdot\underline{r}_{ij}}{r_{ij}^2\rho_i\rho_j}\right)\nabla_i W_{ij}\\ &= \sum_{\substack{i,j=1\\ i<j}}^{N} m_i m_j\left(\frac{p_i}{\rho_i^2}+\frac{p_j}{\rho_j^2} - 8\left(\frac{2\eta_i\eta_j}{\eta_i+\eta_j}\right)\frac{\underline{v}_{ij}\cdot\underline{r}_{ij}}{r_{ij}^2\rho_i\rho_j}\right)(\nabla_i W_{ij} + \nabla_j W_{ji}) = 0,\end{aligned} \tag{29}$$

as from Eq. (28) the identity $\nabla_i W_{ij} = -\nabla_j W_{ji}$ follows. Linear momentum is conserved as a consequence of pressure and viscosity related terms in Eq. (27) being symmetrical with respect to the i and j indexes.

As far as the angular momentum $\underline{P}$ is concerned, it is possible to proceed in a similar manner by calculating its time derivative. We start from Eq. (27) with no external forces and use Eq. (28) to express the kernel gradient:

$$\begin{aligned}\frac{D\underline{P}}{Dt} &= \sum_{i=1}^{N} \frac{D}{Dt}(\underline{r}_i \times m_i \underline{v}_i) = \sum_{i=1}^{n} \underline{r}_i \times m_i \frac{D\underline{v}_i}{Dt} = -\sum_{i,j=1}^{N} \underline{r}_i \times m_i m_j \left(\frac{p_i}{\rho_i^2} + \frac{p_j}{\rho_j^2} - 8\left(\frac{2\eta_i\eta_j}{\eta_i+\eta_j}\right)\frac{\underline{v}_{ij}\cdot\underline{r}_{ij}}{r_{ij}^2\rho_i\rho_j}\right) F(|\underline{r}_{ij}|)\underline{r}_{ij} \\ &= \sum_{\substack{i,j=1 \\ i<j}}^{N} m_i m_j \left(\frac{p_i}{\rho_i^2} + \frac{p_j}{\rho_j^2} - 8\left(\frac{2\eta_i\eta_j}{\eta_i+\eta_j}\right)\frac{\underline{v}_{ij}\cdot\underline{r}_{ij}}{r_{ij}^2\rho_i\rho_j}\right) F(|\underline{r}_{ij}|)\left((\underline{r}_i \times \underline{r}_j) + (\underline{r}_j \times \underline{r}_i)\right) = 0.\end{aligned} \tag{30}$$

Eqs. (29) and (30) prove that the time derivative of both linear and angular momentum for the system of particles is zero when Eq. (27) is used for the momentum equation, showing its conservation properties. We would like to point out that the ability of the model at effectively conserving linear and angular momentum through the time steps of the simulation also depends on the time stepping scheme. Further details on this are given in Section 3.5

High orders of accuracy are usually not achieved with SPH. It is however possible to improve the SPH performance in these regards: Liu et al. [36], Liu and Liu [37] and Oger et al. [38] proposed kernel gradient correction methods to do this. These techniques require additional computational time, as particle-dependent correction matrices that must be recalculated at every time step are employed. Nevertheless, they proved successful at restoring kernel consistency when particles are disordered and/or close to boundaries.

A known problem of these techniques is that the resulting SPH formulations break momentum conservation laws (see Monaghan [13]). In the present work, SPH formulations retaining conservation properties were preferred to others with better consistency properties: this allowed to obtain accurate enough results at reasonable computational cost.

More details regarding SPH conservation properties can be found in Bonet and Lok [39] and in Takeda et al. [40].

Viscosity values to be used in Eq. (26) should be calculated from the constitutive equation of the fluid. For doing this, strain rate tensor components are needed and can be calculated from the following expression, which also has 0th order consistency:

$$\epsilon_i^{\alpha\beta} = -\sum_{j=1}^{n} v_{ij}^{\alpha} \frac{\partial W_{ij}}{\partial x_i^{\beta}} \frac{m_j}{\rho_j}. \tag{31}$$

It is possible to approximate the incompressible fluid behavior with the one of a weakly compressible fluid by using a stiff EOS. An expression of this kind is often used:

$$p = B\left(\left(\frac{\rho}{\rho_0}\right)^{\gamma} - 1\right), \tag{32}$$

where B is a constant having the units of a pressure, ρ_0 is a reference density for the fluid; usually it is the density at zero pressure conditions, γ is a non dimensional parameter, usually ranging from 1 to 7. The Mach number M of the flow can be calculated as:

$$M = \frac{U_{ref}}{c}, \tag{33}$$

where U_{ref} is a reference velocity for the flow and $c = \sqrt{\partial p/\partial \rho}$ is the artificial sound of speed provided by the EOS.

Relative density variations $|\rho - \rho_0|/\rho_0$ scale with $M^2 : B$ can therefore be chosen big enough in order to keep such variations small and to have a good approximation of the incompressible limit. (see Monaghan [4,13]). Typically B is chosen in order to have $M < 0.1$ and, consequently, $|\rho - \rho_0|/\rho_0 < 0.01$.

This kind of approach for setting up SPH computations is usually referred to as Weakly Compressible SPH (WCSPH). We used this approach in the present work as some artificial compressibility for the grains will be introduced in the model of Eq. (13) for stability purposes (see Section 4.1), which leads to the formulation of an EOS for the granular matter.

It is worth mentioning the possibility of using incompressible SPH schemes that do not employ an EOS for computing pressure. Most of them are based on velocity projection methods as in Cummins and Rudman [41] or Hu and Adams [42]. A different approach to incompressible SPH has instead been proposed by Ellero et. al. [43], where Lagrange multipliers are employed in order to enforce particle volume constancy.

3.3. Boundary treatment

The free surface boundary condition ($\underline{\underline{\tau}} = \underline{\underline{0}},\ p = 0$) is implicitly included into the SPH Lagrangian formalism.

Some specific tools need instead to be used in order to enforce no-slip conditions at walls. A straightforward approach is the one of placing particles right on the borders. Boundary particles have zero velocity and pressure and exert repulsive central forces on the real particles they interact with: applications of this method can be found in Monaghan [4] and in Monaghan and Kajtar [34].

A different approach uses ghost particles placed right outside the computational domain boundaries. Possible ways to do this are reported in Ferrari et al. [5] and Liu et al. [44].

In the present work we resorted to the ghost particles approach proposed by Morris et al. [45]. Ghost particles are uniformly placed outside the boundaries to avoid real particles support domain truncation as indicated in Fig. 2. Ghost particles positions and other associated variables are not evolved in time and their spacing is set equal to the initial spacing of real particles. They are given the same total stress as real particles and a fictitious velocity linearly interpolated according to their distance to the boundary with the following expression (refer to Fig. 2 for the meaning of symbols):

$$\underline{v}_j = -\frac{d_j}{d_i}\underline{v}_i. \tag{34}$$

The following expression is used to calculate velocity differences appearing in SPH equations:

$$\underline{v}_{ij} = \beta \underline{v}_i, \tag{35}$$

where the non dimensional β value is chosen so that:

$$\beta = min\left(\beta_{max}, 1 + \frac{d_j}{d_i}\right). \tag{36}$$

Morris et al. [45] obtained good results by choosing $\beta_{max} = 1.5$. As far as the present work is concerned, good results have also been obtained by choosing $\beta_{max} = 1$, which corresponds to assigning zero velocity to every ghost particle.

3.4. Treatment of shocks

Development of shock waves is a common feature in hydrodynamics problems, especially when low dissipations occur. Numerical methods, including SPH, may develop unphysical oscillations around the shocked fronts unless some special treatment is adopted in order to dampen them and to restore correct values ahead and beyond the shock front.

A common approach is the one of adding an artificial viscous term Π_{ij} to the momentum equation:

$$\frac{D\underline{v}_i}{Dt} = \underline{g} - \sum_{j=1}^{n} m_j \left(\frac{p_i}{\rho_i^2} + \frac{p_j}{\rho_j^2} + \Pi_{ij}\right)\nabla_i W_{ij} + \sum_{j=1}^{n} 8\left(\frac{2\eta_i\eta_j}{\eta_i + \eta_j}\right)\frac{(\underline{v}_{ij}\cdot\underline{r}_{ij})\nabla_i W_{ij}}{r_{ij}^2\rho_i\rho_j} m_j \tag{37}$$

Monaghan and Gingold [46] proposed an expression for Π_{ij} capable of increasing the entropy of the system, in order to provide the necessary amount of dissipation:

$$\Pi_{ij} = -\alpha\frac{\overline{h}_{ij}\overline{c}_{ij}}{\overline{\rho}_{ij}}\frac{\underline{v}_{ij}\cdot\underline{r}_{ij}}{r_{ij}^2}, \tag{38}$$

where α is a non dimensional coefficient whose value is usually set below 1 and the overline sign represents arithmetic averages between quantities.

The use of artificial viscosity is sometimes associated to the use of numerical switches that turn off the dissipation terms away from discontinuities as in Price [47]. Other times, artificial viscosity is used regardless of the presence of shocks, as a tool to enhance the stability and the accuracy of the method.

3.5. Time integration

The time stepping scheme used in the present work is a 2nd order accurate scheme based on the symplectic Verlet integrator. Symplectic integrators conserve motion invariants and therefore, coherently with the employed SPH formulations, conserve linear and angular momentum for the system of SPH particles.

Details on the scheme can be found in Kajtar and Monaghan [48] and Monaghan and Kajtar [34]. The scheme can however be summarized with the following list starting from the nth time step:

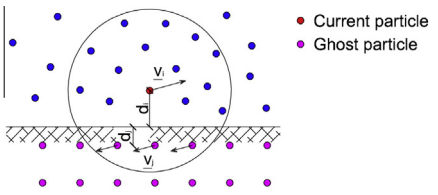

Fig. 2. Scheme for ghost particles approach proposed by Morris et al. [45].

- Evaluate the RHS $D\rho_i/Dt(n)$ of mass conservation equation Eq. (26) based on values of variables at $t = t^n$;
- Make a half Euler time step based on the rates of change $\underline{v}_i(n)$, $D\underline{v}_i/Dt(n-1/2)$ and $D\rho_i/Dt(n)$ to evaluate $\underline{r}_i(n+1/2)$, $\underline{v}_i(n+1/2)$ and $\rho_i(n+1/2)$ respectively;
- Evaluate RHSs $D\rho_i/Dt(n+1/2)$ of mass conservation equation Eq. (26) and $D\underline{v}_i/Dt(n+1/2)$ of momentum equation Eq. (27) based on values of variables at $t = t^{n+1/2}$;
- Make a half Euler time step based on the rates of change $\underline{v}_i(n+1/2)$, $D\underline{v}_i/Dt(n+1/2)$ and $D\rho_i/Dt(n+1/2)$ to evaluate $\underline{r}_i(n+1)$, $\underline{v}_i(n+1)$ and $\rho_i(n+1)$ respectively;

Time step size is constrained by a stability condition, based on both artificial speed of sound and viscous interactions term (see Kajtar and Monaghan [48] and Morris et al. [45]):

$$\Delta t < CFL \cdot min_i\left(\frac{h_i}{c_i}, 0.1\frac{\rho_i h_i^2}{\eta_i}\right), \tag{39}$$

where *CFL* is the Courant-Friedrichs-Lewy number, assumed equal to 0.5 for the 2D simulations carried out in the present work.

4. Model formulation

The set of Eqs. (13) has been solved with SPH. It has been necessary to slightly modify the formulations introduced in Section 3 in order to meet the peculiarities of the equations and the related numerical issues.

The density variable ρ represents the bulk density of the fluid (amount of mass over the unit geometrical volume, including voids),which is related to volume fraction ϕ and density of the granular material ρ_s through Eq. (9). Even if grains are incompressible, volume fraction changes with the inertial number according to Eq. (8): when the granular matter is flowing ($i \neq 0$), ϕ and ρ decrease, making the granular equivalent fluid compressible. It is important to note that, as the constitutive equation is valid for dense regimes, volume fraction should not decrease too much as the material would enter into a disperse regime. The granular matter flowing according to the employed constitutive equation behaves as a weakly compressible fluid even if grains are incompressible and therefore the use of WCSPH is a natural choice: this implies that an EOS needs to be employed to obtain pressures. The model itself contains an EOS relating pressure to density, even though it is not evident from the set of Eqs. (13): in Section 4.1 it will be shown how the issue has been treated in order to solve the equations of the model.

The viscosity provided by Eq. (11) approaches infinity when strain rate approaches zero, that is when the flow moves towards the quasi-static regime. Such condition is computationally unsustainable as time step becomes prohibitively small when viscosity is too large, as it can be easily inferred from Eq. (39). It has therefore been necessary to use a viscosity regularisation method in order to prevent viscosity values from becoming too large. The proposed method, which will be discussed in Section 4.2, takes into account the dependency of viscosity on pressure.

4.1. Grains compressibility

The set of Eqs. (13), in which the grains are supposed to be rigid, represents a closed set of equations, that can be solved to obtain the features of a granular flow of incompressible grains in a dense regime. By using Eqs. (6), (8) and (9), it is possible to prove that the following relation holds:

$$p = \frac{\rho_s^3 \dot{\gamma}^2 d^2 (\phi_{max} - \phi_{min})^2}{(\rho_s \phi_{max} - \rho)^2}. \tag{40}$$

It would be possible, in principle, to use this expression as an EOS to calculate pressure from bulk density ρ. Nevertheless, a major problem caused by the expression is that in static conditions, which always occur when the flow is initiated, $\dot{\gamma} = 0$ and $\rho = \rho_s \phi_{max}$ causing both the numerator and the denominator of Eq. (40) to be zero. The expression is therefore undetermined in such conditions and unstable to handle numerically.

To overcome the problem, an "artificial" compressibility for the grains has been introduced. The SPH approach does not change and remains based on weak compressibility: the "artificial" compressibility of the grains adds up to the "real" one of the granular matter as a whole. The introduction of compressible grains avoids indeterminate forms when calculating pressure, even when close to static conditions at the initiation of flow. On the other hand, the effects of grains compressibility must be small, so that the physics of the problem is not substantially modified: in order to achieve that, the EOS one resorts to must be stiff, causing negligible granular material density ρ_s variations for the range of pressures relevant to the flow under study. The EOS employed to account for grains compressibility is as follows:

$$p = \frac{1}{K_t}\left(\frac{\rho_s}{\rho_{s_0}} - 1\right), \tag{41}$$

where K_t is a compressibility module having the units of the inverse of a pressure and ρ_{s_0} is a reference value for the density of the granular material, representing the density of the material of the grains when they are not confined by any pressure. Such EOS stems from the following compressibility law:

$$Dp = \frac{D\rho_s}{K_t \rho_{s_0}} \tag{42}$$

where D indicates the differentiation operator. Eq. (42) is the common elastic compressibility law linearized about $\rho_s = \rho_{s_0}$. The use of a linearized elastic law is appropriate as only a weak compressibility is being enforced, with ρ_s remaining close to ρ_{s_0}. The use of a non linearized elastic law would provide a logarithmic EOS, which is however less stiff than the linearized one.

The introduction of grain compressibility adds two variables to the list of unknowns: the grain density ρ_s and their size d, which are needed to calculate the inertial number i in Eq. (6). These variables are constant in the system of Eq. (13) where single grains are supposed to be rigid. Two more equations are now needed for solving the system.

The first one is the EOS of Eq. (41), while the other one relates grains diameter variations to pressure or density. The other missing equation can be devised by enforcing mass conservation m for the single grain and assumes the following expression in a 2D case:

$$\frac{d}{d_0} = \sqrt{\frac{\rho_{s_0}}{\rho_s}}, \tag{43}$$

where d_0 is the grains diameter when $\rho_s = \rho_{s_0}$.

Eqs. (41) and (43) are added to the set of Eqs. (13). With this modification the model, featuring weakly compressible grains, has two more unknowns ρ_s and d. It consists of 11 scalar equations and 11 unknowns in a 2D case.

Calculation of ρ_s is necessary at the midpoint of the time stepping scheme listed in Section 3.5, when particle pressures and viscosities are needed to evaluate the RHS of momentum equation Eq. (27).

By using Eqs. (6), (8), (9), (41), (43), it is possible to show that the ρ_s value assumed by particles is given by the solution of the following 3rd order algebraic equation:

$$\rho_s^{*^3} - \left(1 + \frac{2\rho^*}{\phi_{max}} + \frac{\dot{\gamma}^2 \rho_0 K_t (\phi_{max} - \phi_{min})^2 d_0^2}{\phi_{max}^2}\right)\rho_s^{*^2} + \frac{\rho^*(\rho^* + 2\phi_{max})}{\phi_{max}^2}\rho_s^* - \frac{\rho^{*^2}}{\phi_{max}^2} = 0, \tag{44}$$

where superscript "*" indicates variables scaled with the reference density of granular material ρ_{s_0}. The solution of the equation can be found via Newton-Rhapson method or by employing the analytical Cardano's solution. Pressure can then be calculated via Eq. (41) according to the value obtained for ρ_s from the solution of Eq. (44).

When the granular matter is not moving and $\dot{\gamma} = 0$, the equation has two unique solutions, that are $\rho_s = \rho_{s_0}$ and $\rho_s = \rho/\phi_{max}$. The first one is the density of the granular material when it is not confined by any pressure (it happens when there are no body forces, such as gravity, acting on the medium), while the second one is the granular material density resulting from the bulk density of the medium at its maximum packing.

In general, according to the values of the coefficients of the equation, it is possible to have either one real root and two complex roots or three real roots. In the range of values assumed by coefficients during the performed simulations, the equation showed three real roots almost every time. In that case, two of them turned out to be lower than ρ/ϕ_{max} when the granular material was moving. These solutions are unphysical and were discarded, since when the granular material is moving $i > 0$ and $\phi < \phi_{max}$ and that should produce a $\rho_s > \rho/\phi_{max}$ instead. When only one real root was obtained, it turned out to be physically acceptable.

4.2. Viscosity regularisation

SPH methods are normally based on explicit time stepping schemes, where the time step size has an upper bound set by stability conditions, as in Eq. (39). When constitutive equations providing viscosity approaching infinite are used, like the one in the present study, the time step size of Eq. (39) tends to zero. In these cases, it becomes necessary to use a regularisation method to replace the largest values of viscosity with smaller ones that do not produce prohibitively small time steps. The regularised viscosity must however be large enough for the numerical solution to capture the features of the flow.

The method devised to treat the fluid under study stems from the viscosity regularisation approach originally proposed by Papanastasiou [49]. The method, in its original formulation, was applied to a Bingham fluid, whose viscosity can be written in the following way:

$$\eta = \eta_0 + \frac{\tau_y}{\dot{\gamma}}, \tag{45}$$

where η_0 is the residual constant value of viscosity. Regularised viscosity $\hat{\eta}$ has the following expression:

$$\hat{\eta} = \eta_0 + \tau_y \frac{1 - \exp(-m_p \dot{\gamma})}{\dot{\gamma}}, \tag{46}$$

where m_p is a scaling parameters, having the units of a time, used to select how close the regularised model sticks to the real one. Larger values for m_p provide a better approximation of the real constitutive equation, providing on the other hand larger values of viscosity; m_p is usually set up to provide, when $\dot{\gamma} = 0$, a viscosity at least an order of magnitude larger than the residual viscosity η_0. Fig. 3 shows a comparison between the exact viscosity of Bingham model and the one provided by Papanastasiou regularisation method.

The viscosity of the constitutive equation under study can be written in terms of residual viscosity and yield stress. It can be cast in the same form as Eq. (45) with the following choice for η_0:

$$\eta_0(\tau_y, \dot{\gamma}) = \frac{\left(\frac{\mu_2}{\mu_s} - 1\right)\tau_y}{\dot{\gamma} + \frac{i_0}{d_0}\sqrt{\frac{\tau_y}{\mu_s \rho_{s_0}}}}, \tag{47}$$

with τ_y provided by Eq. (12).

As opposite to the Bingham model, η_0 and τ_y are not constant for the considered constitutive equation, depending on both pressure and strain rate tensor modules. However, if the Papanastasiou method were to be straightforwardly used to regularise the viscosity of this model, $\hat{\eta}$ would assume the following expression:

$$\hat{\eta} = \eta_0(\tau_y, \dot{\gamma}) + \tau_y \frac{1 - \exp(-m_p\dot{\gamma})}{\dot{\gamma}}, \tag{48}$$

with η_0 and τ_y provided by Eqs. (47) and (12) respectively. The relative error committed on viscosity $\left(\epsilon_\eta = \left|\frac{\hat{\eta}-\eta}{\eta}\right|\right)$ can then be calculated:

$$\epsilon_\eta(\tau_y, \dot{\gamma}) = \frac{\tau_y(p)\exp(-m_p\dot{\gamma})}{\eta_0(\tau_y, \dot{\gamma})\dot{\gamma} + \tau_y(p)}. \tag{49}$$

In Fig. 4, a qualitative plot of ϵ_η as a function of $\dot{\gamma}$ for different values of the scaling parameter m_p is shown.

It can be seen from Fig. 4 that, at constant strain rate, the use of Papanastasiou method with a constant scaling parameter, originates errors of different magnitudes according to the local yield stress. With a constant scaling parameter, ϵ_η variation with respect to τ_y has the following expression:

$$\frac{\partial \epsilon_\eta}{\partial \tau_y}(m_p = const.) = \frac{\dot{\gamma}\exp(-m_p\dot{\gamma})\left(\eta_0(\tau_y, \dot{\gamma}) - \tau_y\frac{\partial \eta_0}{\partial \tau_y}\right)}{\left(\tau_y + \eta_0(\tau_y, \dot{\gamma})\dot{\gamma}\right)^2}. \tag{50}$$

In the case of Bingham fluid, η_0 and τ_y are constant and m_p is chosen to be constant too. For the constitutive equation under study, as η_0 depends on yield stress (or, equivalently, on pressure), it appears natural to choose a yield stress dependent scaling parameter $m_p(\tau_y)$, rather than a constant one.

In order to establish a criterion for finding an appropriate form for the scaling parameter, the ϵ_η variation with respect to τ_y is written, considering m_p as a function of τ_y:

$$\frac{\partial \epsilon_\eta}{\partial \tau_y} = \frac{\partial \epsilon_\eta}{\partial \tau_y}(m_p = const.) - \epsilon_\eta\dot{\gamma}\frac{dm_p}{d\tau_y}. \tag{51}$$

Eq. (51) provides a first suggestion for the choice of a yield stress dependent scaling parameter, indicating that the error on viscosity regularisation can be lower than in the constant scaling parameter case if $\frac{dm_p}{d\tau_y} > 0$, that is if m_p increases with τ_y.

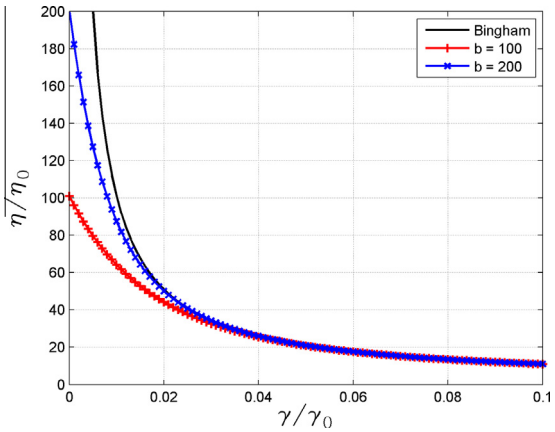

Fig. 3. Viscosity vs strain rate plot for exact Bingham and Papanastasiou models, according to Eqs. (45) and (46). In the plot $\dot{\gamma}_0 = \tau_y/\eta_0,\ m_p = b/\dot{\gamma}_0$.

Furthermore, the dependency of such errors on τ_y can be waived if the RHS of Eq. (51) is made equal to zero. This provides a first order ODE, having the following expression:

$$\frac{dm_p}{d\tau_y} = \frac{\eta_0(\tau_y,\dot{\gamma}) - \tau_y \frac{\partial \eta_0}{\partial \tau_y}}{\tau_y(\tau_y + \eta_0(\tau_y,\dot{\gamma})\dot{\gamma})}, \tag{52}$$

where $\eta_0(\tau_y,\dot{\gamma})$ is provided by Eq. (47).

The boundary condition for this ODE is represented by the value m_0 taken by the scaling parameter m_p at a pre-estabilished level of yield stress τ_0. The maximum viscosity provided by the regularisation method can be obtained by taking the limit of Eq. (48) for $\dot{\gamma} \to 0$:

$$\hat{\eta}_{max}(\tau_y) = \eta_0(\tau_y, 0) + \tau_y m_p(\tau_y), \tag{53}$$

As indicated by Fig. 4 the largest errors occur at the largest values of yield stress for every value of $\dot{\gamma}$: it is therefore convenient to consider the expression of Eq. (53) for the maximum yield stress level τ_0 that is thought to occur during the simulation and then to choose the m_0 value from it, in order to have $\hat{\eta}_{max}(\tau_0)$ at least an order of magnitude larger than the residual viscosity $\eta_0(\tau_y, 0)$.

The ODE of Eq. (52) can be solved numerically for each particle in the SPH simulation. It is easy to find an analytical solution for the equation either if η_0 is constant or weekly dependent on τ_y, so that $\frac{\partial \eta_0}{\partial \tau_y}(\tau_y,\dot{\gamma}) \approx 0$. In this case, the ODE becomes:

$$\frac{dm_p}{d\tau_y} = \frac{\eta_0(\dot{\gamma})}{\tau_y(\tau_y + \eta_0(\dot{\gamma}))} \tag{54}$$

and its solution, with the boundary condition $m_p = m_0$ when $\tau_y = \tau_0$ is:

$$m_p(\tau_y) = m_0 + \frac{1}{\dot{\gamma}} \log\left(1 + \frac{\eta_0(\dot{\gamma})\dot{\gamma}(\tau_y - \tau_0)}{\tau_0(\tau_y + \eta_0(\dot{\gamma})\dot{\gamma})}\right), \tag{55}$$

providing $m_p = m_0 + \eta_0(0)\frac{\tau_y - \tau_0}{\tau_0 \tau_y}$ when $\dot{\gamma}$ approaches zero.

While calculations above are based on the constitutive equation under study for the present work, it is important to remark that the proposed viscosity regularisation method is suitable for any visco-plastic fluid with varying yield stress.

5. Applications

The model equations of Eq. (13), with the extensions described in Section 4, have been solved with SPH in a 2D framework. The model equations and the SPH scheme have been tested on the simple case of a granular flow down an inclined plane, for which the analytical solution is known, and then applied to reproduce a set of existing experimental data on granular columns collapses by Lube et al. [19].

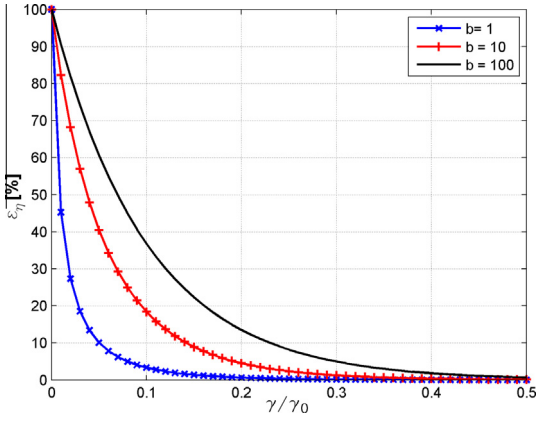

Fig. 4. Plot of relative error on viscosity regularised with the Papanastasiou method for the constitutive equation under study. The three curves differ for the yield stress value τ_y which is in turn set to b orders of magnitude larger than an unitary scaling stress τ_0 ($\tau_y = b\tau_0$). The parameter m_p has been chosen in order to have, when $\dot{\gamma} = 0$, a viscosity on order of magnitude larger than the residual viscosity η_0.

5.1. Granular flow down an inclined plane

The sketch of the problem is displayed in Fig. 5: it is a simple test case of an uniform flow down an inclined plane of indefinite length. In this case, it is easy to find an analytical solution to the equations of Section 2 at the steady state. The velocity profile of the solution has the following expression:

$$v_x(z) = \frac{2i_u}{3d}\sqrt{\phi_u g\cos(\theta)}\left(H^{\frac{3}{2}} - (H-z)^{\frac{3}{2}}\right), \tag{56}$$

with $i_u = i_0(\tan(\theta) - \mu_s)/(\mu_2 - \tan(\theta))$ and ϕ_u calculated from i_u according to Eq. (8).

The parameters of the 1st column (glass beads) of Table 1 have been used in the constitutive equation. Further parameters used in the simulation are listed in Table 2. The value of K_t was chosen in order to have a mach number $M = 0.1$, with a reference velocity equal to the maximum velocity of the flow at the steady state. Periodic boundary conditions were used along the x direction to simulate the indefinite length plane: SPH particles flowing out of the computational domain on the RHS were reintroduced from the LHS, with unchanged values for their physical quantities.

The use of a small value for artificial viscosity ($\alpha = 0.05$) has been found helpful at reducing the errors on velocity computations, which otherwise would have been slightly overestimated by the calculation. The numerical velocity profiles are plotted in Fig. 6.

Pressure distribution is not significantly affected by artificial viscosity. Fig. 7 shows the pressure profile for the simulation with artificial viscosity $\alpha = 0$. In the case of $\alpha = 0.05$ an essentially identical plot is obtained. Pressure distribution is the one of a fluid at rest, and it is reproduced by SPH fairly well.

Particles disposition at the steady state for the simulation is shown in Fig. 8.

5.2. Granular columns collapses

Lube et al. [19] performed a series of experiments consisting in the sudden release of cylindrical columns of granular material over a flat surface by raising the containing cylinder. The material radially collapsed forming axisymmetrical piles. Motion of the granular material was recorded with a high frame rate camera and the geometry of the final deposit was measured. Several materials were used, including sand, salt and rice and different geometries for the columns were tested. A sketch of the experimental setup and parameters used by Lube et al. [19] can be found in Fig. 9.

Starting from dimensional analysis considerations, a scaling law was sought between the final geometry of the deposit described by the parameter $r_\infty - r_0/r_0$ and the initial shape of the column described by the aspect ratio $a = H_0/r_0$ (meanings of symbols can be found in Fig. 9):

$$\frac{r_\infty - r_0}{r_0} = f(a). \tag{57}$$

Measurements on the final geometry of the deposit could be interpolated with the following functions, which turned out to be independent from the material:

$$\begin{aligned} f(a) &= 1.24a \quad \text{for} \quad a < 1.7, \\ f(a) &= 1.6a^{1/2} \quad \text{for} \quad a > 1.7. \end{aligned} \tag{58}$$

Each function above corresponds to a different regime for the behavior of the column during the collapse. In the first case, that is $a < 1.7$, two zones formed on the free surface of the column: a flowing outer one and a static inner one. In the second case, that is $a > 1.7$, the entire free surface of the column started to flow immediately as soon as the containing cylinder was removed. Lube et al. [19] identified different flow patterns within the two regimes above.

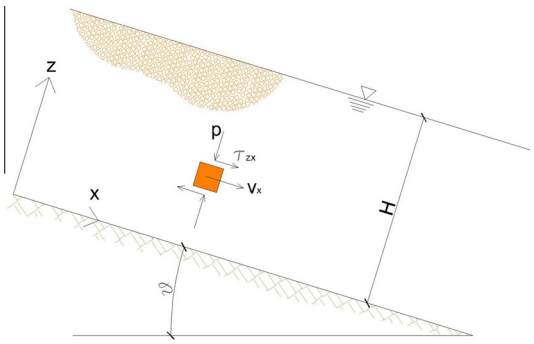

Fig. 5. Sketch for uniform granular flow down an inclined plane.

Table 2
Parameters used for the simulation of granular flow down an inclined plane. N is the number of particles employed in the simulation, dp is their initial spacing and h is the smoothing length.

H (m)	0.1
θ (°)	25.0
ρ_{s_0} (kg/m^3)	800
K_t (Pa^{-1})	$1.5 \cdot 10^{-5}$
τ_0 (Pa)	190
m_0 (s)	1
$\dot{\eta}_{max}$ (Pa·s)	190.3
N	800
dp (mm)	5
h (mm)	6.5

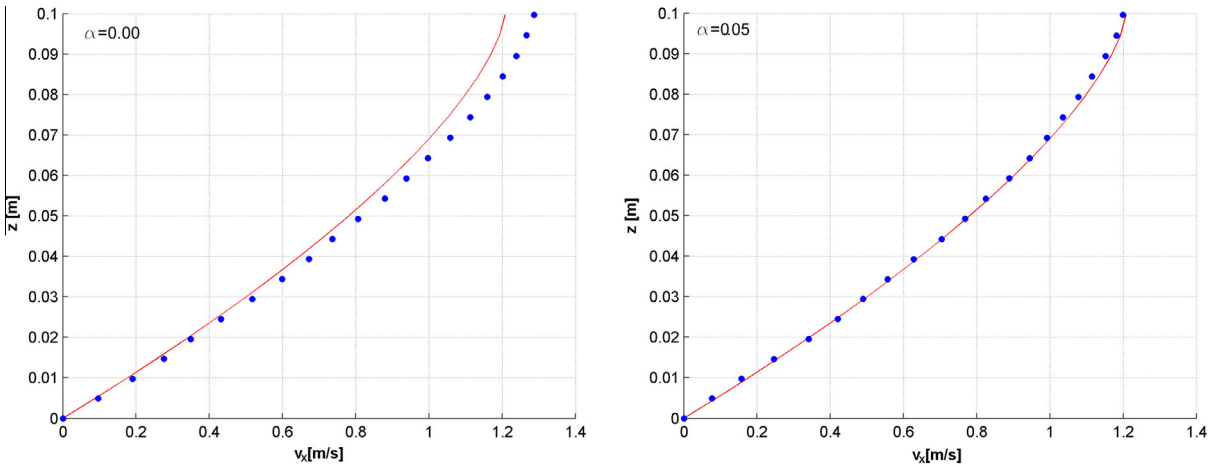

Fig. 6. Steady state velocity profiles for the simulation of granular flow down an inclined plane. The continuous line represents the analytical solution. No artificial viscosity ($\alpha = 0$) has been used for the plot on the left, while artificial viscosity with $\alpha = 0.05$ has been used for the plot on the right. Steady state was reached after about 6.50 s of simulated time in both cases.

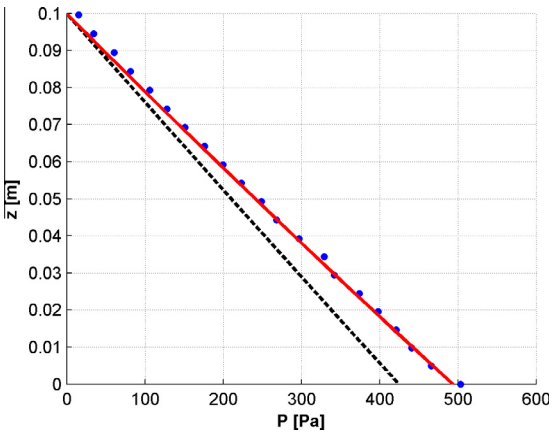

Fig. 7. Steady state pressure profiles for the simulation of granular flow down an inclined plane. The dashed line represents the analytical solution for incompressible grains. The continuous line represents the analytical solution for compressible grains with EOS Eq. (41). No artificial viscosity ($\alpha = 0$) was used in the simulation.

The experiments reproduced with SPH involved sand with $d = 0.32$ mm, $\rho_{s_0} = 2600\,\mathrm{Kg/m^3}$ and an initial radius of the column equal to $r_0 = 9.72$ *cm*. For the SPH simulations, the parameters for the constitutive equation were set to the values indicated by the 3rd column of Table 1. Further parameters used in the simulations are listed in Table 3. The value of K_t was chosen in order to have a mach number $M = 0.1$, with a reference velocity $U_{ref} = \sqrt{gH}$. No artificial viscosity was used in the simulations.

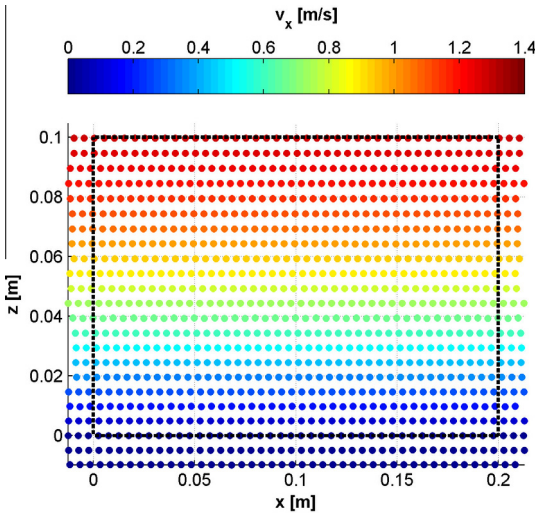

Fig. 8. Steady state particles disposition for the simulation of granular flow down an inclined plane. Particles are color coded according to v_x. The dashed black line indicates the fluid flow region. Particles under the line are boundary particles, while the ones on the sides are standard particles copied in order to enforce periodic boundary conditions.

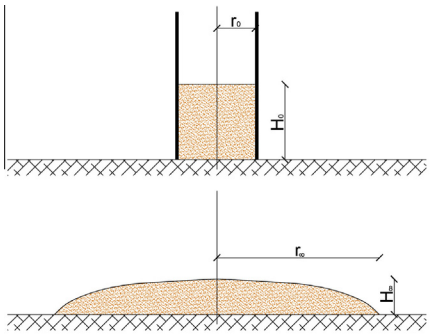

Fig. 9. Granular columns collapses: sketch of experimental setup and parameters definition [19].

It appears reasonable to assume the initial pile height H_0 as a proper scaling length for the granular columns collapses experiments. In this case, as all the reproduced experiments involve values of $H_0/d > 50$, it follows from Section 2.1 that the simple Eq. (7) with $i_0 = 2.65$ can be used to calculate μ, at the price of a negligible error on the estimation of the coefficient.

As viscosity regularisation is being used, it is impossible to exactly reproduce near stop conditions, as viscosity always has a finite value in the numerical simulations. For this reason, after the collapse of a granular column was complete, its front would still keep moving, however having a speed at least three orders of magnitude smaller than during the collapse.

Due to the implementation of a weak compressibility model for the grains with Eq. (41), pressure oscillations when the flow is close to static conditions are strongly reduced. As a consequence, they have a negligible influence on the ability of the model at reproducing stopping flow conditions.

Front advancement in time is displayed in Fig. 10 for the simulations listed in Table 3.

Figs. 11 and 12 show particles disposition at various instants for the simulations with aspect ratio $a = 0.90$ and $a = 2.75$ respectively.

Scalings obtained from SPH simulations were compared with the ones found by Lube et al. [19] for experiments with sand columns. Results are shown in Fig. 13.

The SPH simulations have been able to reproduce the different behavior of the flow during the collapse in the two regimes, as observed by Lube et al. [19]. Furthermore, Fig. 13 shows that a good agreement exists between numerical and experimental results indicating that the SPH model is able to correctly reproduce this kind of granular flow.

SPH simulations with larger values of the aspect ratio ($a > 3.0$) were performed: the agreement with the experimental data was not satisfactory. Nevertheless, in those cases a consistent number of particles located on the front of the collapse

Table 3
Parameters used for the simulation of granular columns collapses. N is the number of particles employed in the simulation, dp is their initial spacing and h is the smoothing length.

Id.	a ()	H_0 (mm)	K_t (Pa^{-1})	τ_0 (Pa)	m_0 (s)	$\hat{\eta}_{max}$ (Pa·s)	N	dp (mm)	h (mm)
1	0.19	18.5	$9.0 \cdot 10^{-5}$	177	1.2	215	2500	1.20	1.56
2	0.55	53.5	$5.3 \cdot 10^{-5}$	483	1.4	684	2200	2.20	2.86
3	0.90	87.5	$4.1 \cdot 10^{-5}$	795	1.2	961	1900	3.02	3.93
4	1.60	155.5	$3.1 \cdot 10^{-5}$	1414	1.4	2003	2900	3.24	4.21
5	2.75	267.3	$2.4 \cdot 10^{-5}$	2415	1.6	3911	2300	4.86	6.32
6	3.00	291.6	$2.2 \cdot 10^{-6}$	2660	1.6	4292	2500	4.86	6.32

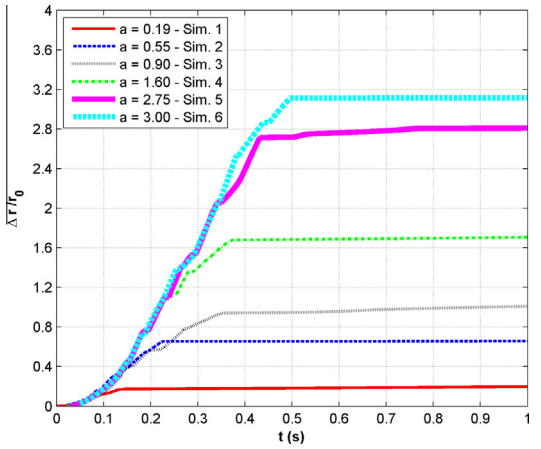

Fig. 10. Front position in time for granular columns collapse simulations. Δr Indicates front advancement with respect to initial position before the collapse of the column.

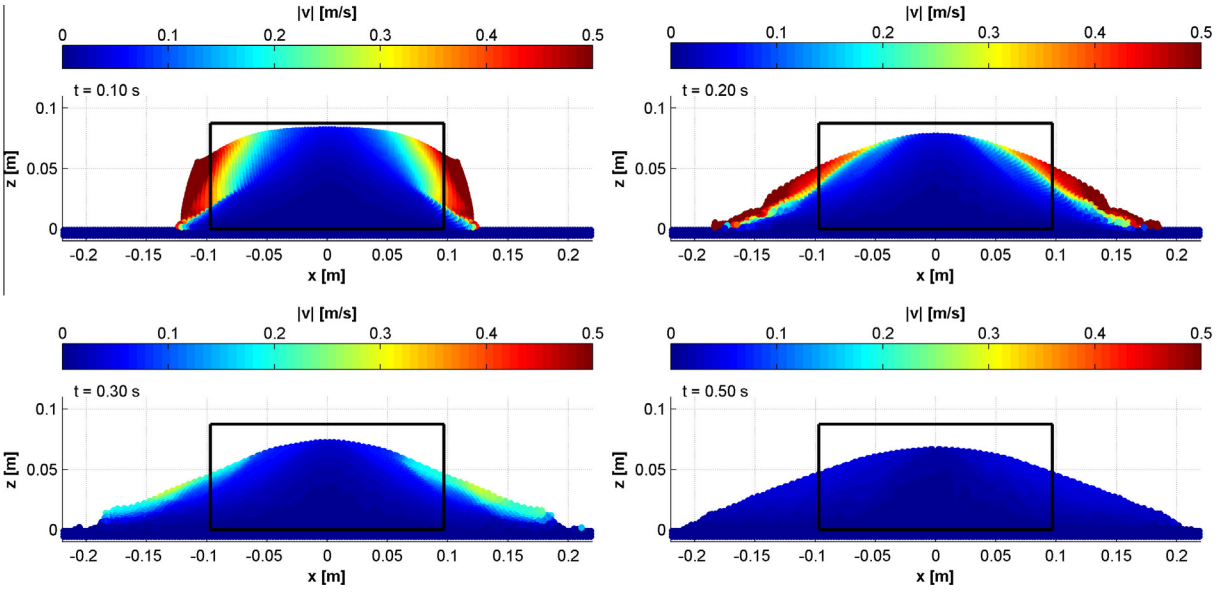

Fig. 11. Particles disposition for the granular columns collapses simulation with $a = 0.90$. Particles are color coded according to velocity module. Reference time of simulation is displayed on each picture. The black frame is used to keep track of initial shape of the pile.

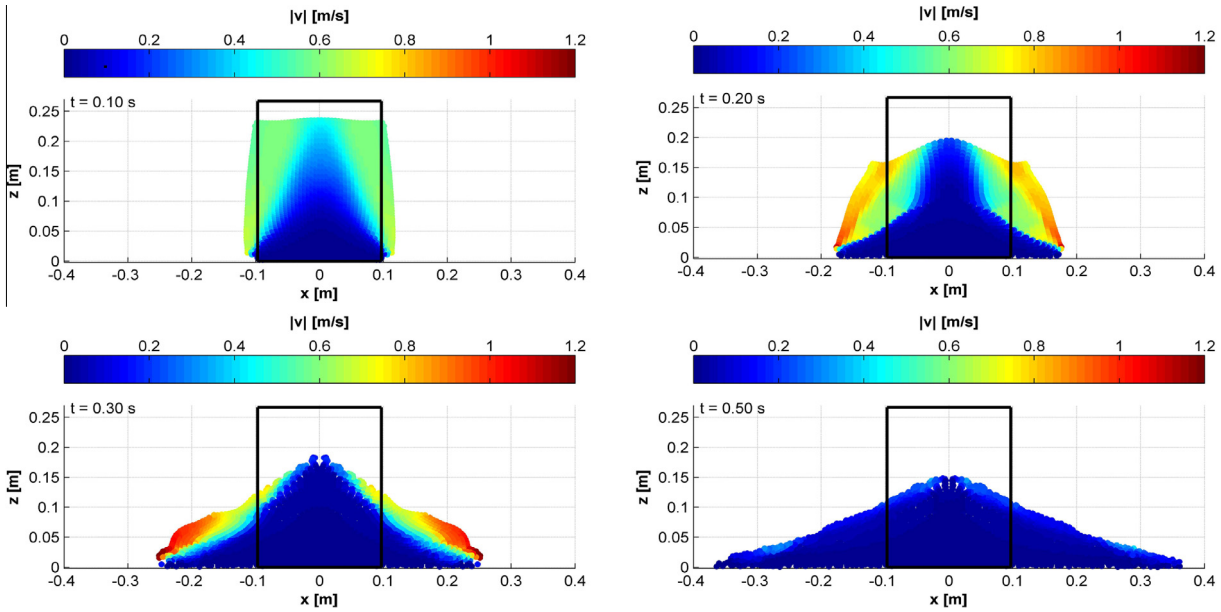

Fig. 12. Particles disposition for the granular columns collapses simulation with $a = 2.75$. Particles are color coded according to velocity module. Reference time of simulation is displayed on each picture. The black frame is used to keep track of initial shape of the pile.

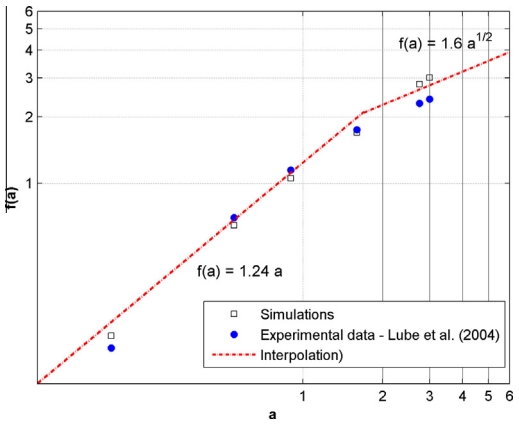

Fig. 13. Scalings from numerical simulations compared with scalings from Lube et al. [19] for sand granular columns collapses.

showed large values for the inertial number ($i > 0.3$), indicating that the material was flowing outside of the dense regime, for which the constitutive equation was devised.

6. Conclusions

This paper presented a SPH model for solving granular flows problems in a dense regime. The model features a constitutive equation proposed by Pouliquen et al. [17] and Jop et al. [18] which is specific to the dense regime of flow.

A weakly compressible SPH approach (WCSPH) has been used: it reflects the features of the constitutive equation which predicts a diminishing granular packing as the intensity of the flow increases.

It has been necessary to introduce a weak compressibility of the grains, in order to bypass pressure estimation problems arising when close to near static conditions. This introduced further unknowns to the problem and the algorithm required the solution of a third order algebraic equation at each time step and for every particle in order to compute the density of the granular material.

A new viscosity regularisation method has been proposed in order to model near static and stopping flow conditions. The proposed method can be used with any visco-plastic model with varying yield stress and requires the solution of first order ODEs to compute the regularised viscosity. The method proved to be capable of reproducing near static and stopping flow conditions within reasonable approximation.

The SPH model has been validated by confronting its results with the known analytical solution of the uniform flow down an inclined plane and by reproducing experimental data of granular columns collapses by Lube et al. [19]. Within the dense regime of flow, the agreement with known solutions and observed data was satisfactory and the model proved to be capable of properly handling the features of the constitutive equation, such as space varying viscosity, pressure dependent yield stress and singular behavior at static conditions.

As far as possible extensions of the model are concerned, it would be interesting to upgrade the model by featuring constitutive equations valid for the so-called collisional [22] regime of flow, in which grains are flowing more far apart than in the dense regime and flow intensity is generally higher. Validation of the model could still be performed on the experimental data by Lube et al. [19] for larger values of the aspect ratio a.

Acknowledgments

Lorenzo Minatti is grateful to the Italian Fire Department who supported the research that led to the development of the present work.

References

[1] C. Hirt, B. Nichols, Volume of fluid (VOF) method for the dynamics of free boundaries, J. Comput. Phys. 39 (1981) 201–225.
[2] R. Gingold, J. Monaghan, Smoothed particle hydrodynamics – theory and application to non-spherical stars, Mon. Not. R. Astron. Soc. 181 (1977) 375–389.
[3] L. Lucy, A numerical approach to the testing of the fission hypothesis, Astron. J. 82 (1977) 1013–1024.
[4] J. Monaghan, Simulating free surface flows with SPH, J. Comput. Phys. 110 (1994) 399–406.
[5] A. Ferrari, M. Dumbser, E.F. Toro, A. Armanini, A new 3d parallel SPH scheme for free surface flows, Comput. Fluids 38 (2009) 1203–1217.
[6] D. Violeau, R. Issa, Numerical modelling of complex turbulent free-surface flows with the SPH method: an overview, Int. J. Numer. Methods Fluids 53 (2007) 277–304.
[7] M.X. Rodriguez-Paz, J. Bonet, A corrected smooth particle hydrodynamics method for the simulation of debris flows, Numer. Methods Partial Differ. Equ. 20 (2004) 140–163.
[8] D. Laigle, P. Lachamp, M. Naaim, SPH-based numerical investigation of mudflow and other complex fluid flow interactions with structures, Comput. Geosci. 11 (2007) 297–306.
[9] A. Pasculli, L. Minatti, N. Sciarra, E. Paris, SPH modeling of fast muddy debris flow: numerical and experimental comparison of certain commonly utilized approaches, Ital. J. Geosci. 132 (2013) 350–365.
[10] L. Minatti, A. Pasculli, SPH numerical approach in modelling 2d muddy debris flow, in: Italian Journal of Engineering Geology and Environment – 5th International Conference on Debris-Flow Hazards Mitigation Mechanics, Prediction and Assessment, Padova (Italy), 15–17 June 2011.
[11] H.H. Bui, R. Fukagawa, K. Sako, S. Ohno, Lagrangian meshfree particles method (SPH) for large deformation and failure flows of geomaterial using elastic-plastic soil constitutive model, Int. J. Numer. Anal. Methods Geomech. 32 (2008) 1537–1570.
[12] J.J. Monaghan, Smoothed particle hydrodynamics, Annu. Rev. Astron. Astrophys. 30 (1992) 543–574.
[13] J. Monaghan, Smoothed particle hydrodynamics, Rep. Prog. Phys. 68 (2005) 1703–1758.
[14] G. Liu, M. Liu, Smoothed Particle Hydrodynamics: A Meshfree Particle Method, World Scientific, 2003.
[15] D. Violeau, Fluid Mechanics and the SPH Method: Theory and Applications, Oxford University Press, 2012.
[16] P. Richard, M. Nicodemi, R. Delannay, P. Ribiere, D. Bideau, Slow relaxation and compaction of granular systems, Nat Mater 4 (2005) 121–128.
[17] O. Pouliquen, C. Cassar, P. Jop, Y. Forterre, M. Nicolas, Flow of dense granular material: towards simple constitutive laws, J. Stat. Mech.: Theory Exp. 07 (2006) P07020.
[18] P. Jop, Y. Forterre, O. Pouliquen, A constitutive law for dense granular flows, Nature 441 (2006) 727–730.
[19] G. Lube, H.E. Huppert, R.S.J. Sparks, M.A. Hallworth, Axisymmetric collapses of granular columns, J. Fluid Mech. 508 (2004) 175–199.
[20] T. Poschel, T. Schwager, Computational Granular Dynamics, Springer-Berling, Heidelberg, New York, 2005.
[21] L.D. Landau, E.M. Lifshitz, Course of Theoretical Physics, Fluid Mech, Vol. 6, Butterworth-Heinemann, 1987.
[22] G.D.R. Midi, On dense granular flows, Eur. Phys. J. E 14 (2004) 341–365.
[23] I. Goldhirsch, Rapid granular flows, Annu. Rev. Fluid Mech. 35 (2003) 267–293.
[24] F. da Cruz, S. Emam, M. Prochnow, J.-N. Roux, F.m.c. Chevoir, Rheophysics of dense granular materials: discrete simulation of plane shear flows, Phys. Rev. E 72 (2005) 021309.
[25] P. Jop, Y. Forterre, O. Pouliquen, Crucial role of sidewalls for granular surface flows: consequences for the rheology, J. Fluid Mech. 541 (2005) 167–192.
[26] Y. Forterre, O. Pouliquen, Flows of dense granular media, Annu. Rev. Fluid Mech. 40 (2008) 1–24.
[27] M.J. Woodhouse, A.J. Hogg, A.A. Sellar, Rapid granular flows down inclined planar chutes. Part 1, J. Fluid Mech. 652 (2010) 427–460.
[28] V. Kumaran, Dense granular flow down an inclined plane: from kinetic theory to granular dynamics, J. Fluid Mech. 599 (2008) 121–168.
[29] O. Pouliquen, Scaling laws in granular flows down rough inclined planes, Phys. Fluids 11 (3) (1999) 542–548.
[30] O. Pouliquen, Y. Forterre, Friction law for dense granular flows: application to the motion of a mass down a rough inclined plane, J. Fluid Mech. 453 (2002) 133–151.
[31] Y. Forterre, O. Pouliquen, Long surface wave instability in dense granular flows, J. Fluid Mech. 486 (2003) 21–50.
[32] T. Borzsonyi, R. Ecke, Flow rule of dense granular flows down a rough incline, Phys. Rev. E 76 (031301) (2007) 1–10.
[33] H. Wendland, Piecewise polynomial, positive definite and compactly supported radial functions of minimal degree, Adv. Comput. Math. 4 (1995) 389–396, http://dx.doi.org/10.1007/BF02123482.
[34] J. Monaghan, J. Kajtar, SPH particle boundary forces for arbitrary boundaries, Comput. Phys. Commun. 180 (2009) 1811–1820.
[35] P.W. Cleary, Modelling confined multi-material heat and mass flows using SPH, Appl. Math. Model. 22 (1998) 981–993.
[36] W. Liu, S. Jun, Y. Zhang, Reproducing kernel particle methods, Int. J. Numer. Methods Fluids 20 (1995) 1081–1106.
[37] M. Liu, G. Liu, Restoring particle consistency in smoothed particle hydrodynamics, Appl. Numer. Math. 56 (2006) 19–36.
[38] G. Oger, M. Doring, B. Alessandrini, P. Ferrant, An improved SPH method: towards higher order convergence, J. Comput. Phys. 225 (2007) 1472–1492.
[39] J. Bonet, T.-S. Lok, Variational and momentum preservation aspects of smooth particle hydrodynamic formulations, Comput. Methods Appl. Mech. Eng. 180 (1999) 97–115.
[40] H. Takeda, S.M. Miyama, M. Sekiya, Numerical simulation of viscous flow by smoothed particle hydrodynamics, Prog. Theor. Phys. 92 (1994) 939–960.

[41] S. Cummins, M. Rudman, An SPH projection method, J. Comput. Phys. 152 (1999) 584–607.
[42] X.Y. Hu, N.A. Adams, An incompressible multi-phase SPH method, J. Comput. Phys. 227 (2007) 264–278.
[43] M. Ellero, M. Serrano, P. Espanol, Incompressible smoothed particle hydrodynamics, J. Comput. Phys. 226 (2007) 1731–1752.
[44] M. Liu, G. Liu, K. Lam, Investigations into water mitigation using a meshless particle method, Shock Waves 12 (2002) 181–195.
[45] J. Morris, P. Fox, Y. Zhu, Modeling low reynolds number incompressible flows using SPH, J. Comput. Phys. 136 (1997) 214–226.
[46] J. Monaghan, R. Gingold, Shock simulation by the particle method SPH, J. Comput. Phys. 52 (1983) 374–389.
[47] D. Price, Modelling discontinuities and kelvinhelmholtz instabilities in SPH, J. Comput. Phys. 227 (24) (2008) 10040–10057.
[48] J. Kajtar, J. Monaghan, SPH simulations of swimming linked bodies, J. Comput. Phys. 227 (2008) 8568–8587.
[49] T. Papanastasiou, Flows of materials with yield, J. Rheol. 31 (5) (1987) 385–404.